Geophysical Journal International

Geophys. J. Int. (2015) **200,** 1336–1346 doi: 10.1093/gji/ggu477

GJI Geomagnetism, rock magnetism and palaeomagnetism

On the applicability of Backus' mantle filter theory

K. J. Pinheiro,[1,2] A. Jackson[3] and H. Amit[2]

[1] *Geophysics Department, Observatório Nacional, Rio de Janeiro, CEP:*20921-400*, Brazil. E-mail: kpinheiro@on.br*

[2] *CNRS, Université de Nantes, Nantes Atlantiques Universités, UMR CNRS* 6112*, Laboratoire de Planétologie et de Géodynamique,* 2 *rue de la Houssinière, F-*44000 *Nantes, France*

[3] *Institute of Geophysics, ETH Zurich, Zurich* 8092*, Switzerland*

Accepted 2014 December 11. Received 2014 December 10; in original form 2014 February 19

SUMMARY

Geomagnetic jerks are sudden changes of trend in the geomagnetic secular variation. The Earth's mantle behaves as a filter for the jerks, causing a delayed and a smoothed signal at the Earth's surface. Backus' mantle filter theory relies on approximating the impulse response function (IRF) of the mantle by a Gaussian. The advantage of this theory is the linear relation between jerks' delay times and the mantle electrical conductivity, as expressed by kernels. However, the limitations of this theory arise when negative delay and/or smoothing times occur. The applicability of the mantle filter theory is examined by analysing the validity of the Gaussian as an approximation for the composite IRF (CIRF) at a given location. We show that the electrical conductivity of the lower mantle is mostly responsible for the jerk delay time. Alternating sign CIRFs might cause negative delay and/or smoothing times which prevents the use of the mantle filter theory. Adequate/inadequate Gaussian approximations to the CIRFs give small/large differences in the convolved jerk occurrence times. Most observatories yield positive time constants, but in most cases the difference in the jerk occurrence times exceeds 0.5 yr.

Key words: Geomagnetic induction; Magnetic and electrical properties; Rapid time variations.

1 INTRODUCTION

The Earth's magnetic field is comprised of contributions from internal sources originating in the liquid outer core and crust and external fields generated in the ionosphere and magnetosphere where the solar wind interacts with the magnetic field of the Earth. Temporal fluctuations of the external field range from milliseconds to a few decades, with the shortest periods related to the variations of the solar magnetic field. Variations over time-scales ranging from a few years to millions of years are due to the changes in the internal magnetic field and are called secular variation (SV).

Geomagnetic jerks are the shortest observed variations of the core field and are usually represented by an impulse in the third time derivative of a component of the magnetic field (Courtillot *et al.* 1978; Malin & Hodder 1982; Mandea *et al.* 2000; Olsen & Mandea 2007). The physical origin of these rapid events has been the focus of many studies in the past decade (Bloxham *et al.* 2002; Holme & de Viron 2005; Olsen & Mandea 2008; Wardinski *et al.* 2008; Chulliat *et al.* 2010; Silva & Hulot 2012; Holme & de Viron 2013). Geomagnetic jerks of worldwide extent occurred in 1969, 1978 and 1991, while some localized events happened in 1913, 1925 and 2003. Regional/global jerks distinction may be obtained by examining the consistency of the occurrence patterns (Brown *et al.* 2013). Global jerks do not occur at the same time on the Earth's surface: some observatories registered early jerk arrivals, while others detected late jerk occurrences. The difference between jerk arrivals in different magnetic observatories is termed the *jerk differential delay* (Pinheiro & Jackson 2008) and is typically on the order of 2 yr. If the jerk corresponds to a simultaneous event at the core-mantle boundary (CMB), the differential delay observed at the Earth's surface is likely the effect of the mantle's electrical conductivity.

The electrical conductivity of the mantle has been the subject of much debate in the last decade, especially after the discovery of the post-perovskite phase transition (Murakami *et al.* 2004). Ohta *et al.* (2008) performed direct measurements of the post-perovskite electrical conductivity at D″ conditions. Their measurements indicate a D″ conductance of 4×10^7 S, corresponding to a uniform electrical conductivity of about 140 S m^{-1}.

Temporal variations of the external and internal geomagnetic fields have also been used in attempts to constrain physical properties of the deep Earth. One of the earliest applications of induction to obtain information about the electrical conductivity was that of Lahiri & Price (1939) who considered the general theory for any radially varying electrical conductivity in a spherical geometry. They applied their formal solution to solar diurnal and storm-time variations to estimate the mantle's electrical conductivity up to 1000 km depth. Olsen (1998) used two different external field sources to

evaluate induction responses in Europe: geomagnetic daily variations generated in the ionosphere and variations caused by the decay of magnetic storms in the magnetosphere (periods between 3 hr and 30 d). He found a monotonic increase of the electrical conductivity from 0.01 S m^{-1} at 200 km depth to about 1.4 S m^{-1} below 1000 km depth. Olsen (1999) used longer periods (from 30 d to 1 yr) to estimate the electrical conductivity in deeper mantle layers. Induction responses were calculated using daily mean values at 42 magnetic observatories. He inferred an increase of the electrical conductivity from 800 km depth ($\sigma = 2$ S m^{-1}) to 2000 km ($\sigma = 3$–10 S m^{-1}). In general, induction studies converge to similar models of the mantle's electrical conductivity roughly from 0.01 S m^{-1} in the upper mantle to 0.5 S m^{-1} at around 1400 km depth (Olsen 1998, 1999; Kuvshinov *et al.* 2005; Kuvshinov & Olsen 2006; Semenov & Kuvshinov 2012). More recently, Tarits & Mandea (2010) used 32 yr of magnetic monthly mean data and found average values from 6 to 7 S m^{-1} in the depth range of 900–1500 km. The ability of induction studies to unravel the electrical conductivity of deep lower mantle layers is limited because the skin depth, that is the characteristic length over which electromagnetic field attenuates by an e-fold (Constable 2007), is shallow. In addition, transient induction in the metallic core caused by magnetospheric field variations must be included in accurate portrayals of the near-Earth magnetic environment (Velímský & Finlay 2011).

In order to explore the electrical conductivity of the lowermost mantle, studies involving the core field were developed. Runcorn (1955) discussed the theory of the diffusion of the magnetic field by considering the mantle as an infinite sheet of uniform thickness and conductivity. He applied a step-like signal at the bottom of the slab and evaluated the magnetic signal observed at the top. McDonald (1957) used the geomagnetic SV and estimated the mantle electrical conductivity as 1 S m^{-1} at about 1000 km depth and about 100 S m^{-1} in the lowermost mantle. Achache *et al.* (1980) performed the same calculation as Runcorn (1955), but they used instead a ramp-function at the bottom of the slab (2000 km). Based on the geomagnetic jerk of 1969 they calculated responses for different values of electrical conductivity and obtained 60 S m^{-1} for the mean conductivity of the slab which corresponds to a conductance of 1.2×10^8 S. Alexandrescu *et al.* (1999) modelled the 1969 jerk as a pure singularity at the CMB and evaluated the effect caused by a uniformly conducting mantle. Their estimated electrical conductivity is less than 10 S m^{-1} on average assuming a uniform conducting lower mantle 2000 km thick and an insulating upper mantle. Nagao *et al.* (2003) also solved the diffusion equation in the mantle for an abrupt change occurring simultaneously at the CMB. They argued that the later arrival of jerks in South Africa and South Pacific Ocean may be explained by higher conductivities beneath these regions. In order to explain these jerk delay times, the conductivity beneath the South Africa and South Pacific Ocean would be greater than 200 S m^{-1}.

The relation between mantle's electrical conductivity and jerk delay times was first established by Backus (1983). He developed a theory that considers the mantle as a linear, causal and time invariant filter. The input signal is represented by a geomagnetic jerk at the CMB, the mantle as the filter and the output as the jerk observed at the Earth's surface. The effect of the mantle filter is to delay and smooth the original signal generated in the core, as shown by the synthetic example in Fig. 1. Pinheiro & Jackson (2008) applied Backus' mantle filter theory (Backus 1983) and demonstrated that a simple 1-D mantle conductivity model is able to produce differential jerk delay times at the Earth's surface and even different patterns for different jerk events.

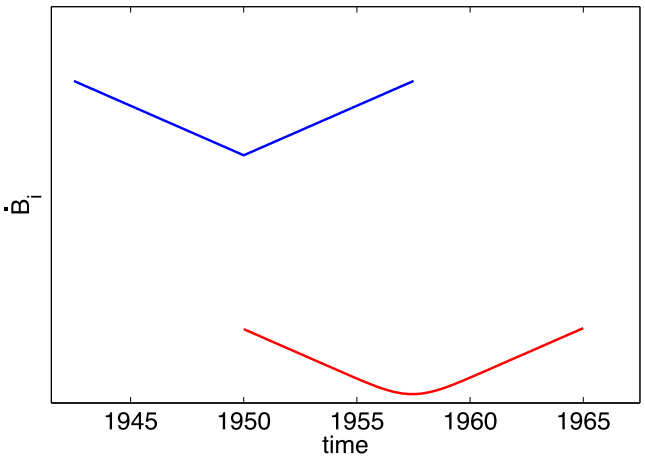

Figure 1. Schematic illustration of a time-serie of the secular variation of a magnetic field component B_i and the delay and smoothing caused by an electrically conducting mantle. The blue curve represents a geomagnetic jerk at the CMB and the red curve represents the output signal at the Earth's surface.

Backus' mantle filter theory relies on a low-frequency approximation which simplifies the formalism, since the impulse response function (IRF, see Section 2.1) $F(t)$ of the filter can be represented by a Gaussian probability distribution function (PDF):

$$F(t) \simeq \frac{1}{\sqrt{2\pi(\beta_2)^2}} \exp\left(\frac{-(t-\tau)^2}{2(\beta_2)^2}\right), \quad (1)$$

where τ is the mean of the Gaussian corresponding to the delay time and $(\beta_2)^2$ is the variance that represents the jerk smoothing time. The delay time is defined as the time difference between jerk occurrences at the Earth's surface and the CMB. The consequence of the Gaussian approximation is the linear relation between the jerk delay time $\tau(\ell)$ and the radial profile of the electrical conductivity $\sigma(r)$ in the spherical harmonic domain (see Section 2.2). However, there are some limitations on this approximation when representing an IRF at a given location termed Composite IRF (CIRF, Pinheiro & Jackson 2008). In CIRFs the delay and smoothing time constants might be negative due to mixing of harmonics. In that case the Gaussian approximation to the CIRF and the linear relation between $\tau(\ell)$ and $\sigma(r)$ are no longer valid.

The causality condition requires jerks arrival at the Earth' surface after they are generated in the core ($\tau > 0$). Jerks may be represented by an impulse in the third time derivative of a magnetic field component in the core, or as a V-shaped SV. Therefore, the smoothing time of the jerk in the core would be null. Because of the mantle's filter effect, there is a smoothing of the V-shaped SV, as shown in Fig. 1. At the Earth's surface the smoothing time may also be termed jerk duration (Nagao *et al.* 2003), which means the period that the SV takes to change completely from one linear trend to another. Thus, there would be no reasonable physical meaning for negative smoothing time since the jerk at the surface cannot be more instantaneous than its assumed behaviour in the core.

The calculation of the IRF is based on the exact solution of the diffusion equation in spherical coordinates which directly stems from Maxwell's equations in a solid conductive mantle. However, based on the IRF alone, the delays and smoothing times can only be calculated numerically, not analytically. The most advantageous aspect of the theory of Backus (1983) is the derived linear relation between any radial mantle electrical conductivity profile and jerk delay times. These kernels provide insight on the sensitivity of the

Table 1. Notation of the variables used in this paper: symbols are written as functions of the Earth's radius (r), time (t), frequency (ω), harmonic degree (ℓ), colatitude (θ) and longitude (ϕ).

Symbol	Function of	Meaning
$\mathcal{P}$	r, θ, ϕ, t	Poloidal scalar
p_ℓ^m	r, t	Poloidal scalar coefficient representing jerk amplitude at CMB
$\mathcal{G}$	ℓ	Geometrical filter
F	ℓ, t	Impulse response function
$\tilde{F}$	ℓ, ω	Transfer function
τ	ℓ	Delay time
$(\beta_2)^2$	ℓ	Smoothing time
$F_{\rm loc}$	ℓ, θ, ϕ, t	Composite impulse response function
$\tau_{\rm loc}$	ℓ, θ, ϕ	Local delay time
$(\beta_2)^2_{\rm loc}$	ℓ, θ, ϕ	Local smoothing time
$\mathcal{A}$	ℓ, θ, ϕ	Local jerk total amplitude
α	ℓ, θ, ϕ	Normalized amplitude ratio
κ	ℓ, r	Kernel relating the delay time with electrical conductivity profile
σ	r	Electrical conductivity profile
σ_c		Electrical conductivity value at the CMB
γ		Electrical conductivity power constant

mantle to a given electrical conductivity distribution in terms of producing jerk delay times. In particular, it may indicate at which region of the mantle the filtering effect is most prominent. Overall, understanding the applicability and limitations of Backus' mantle filter theory is important in order to advance the inference of the mantle electrical conductivity by geomagnetic SV observations and may therefore improve the knowledge of the internal structure and dynamics of the deep Earth.

Pinheiro & Jackson (2008) used Backus' theory to show that a 1-D mantle conductivity model can generate jerk differential delay times at the Earth's surface. However, they did not explore the applicability and limitations of this theory. Here, we calculate and interpret kernels, which relate a radial electrical conductivity profile with the jerk delay times. We explore the applicability of Backus' mantle filter theory and quantify under which conditions it might fail. Finally, we also quantify how the Gaussian approximation could affect the calculated jerk delay times.

The paper is outlined as follows: in Section 2 we present the theory for the time constants and for the kernels. In Section 3 we test the validity of assuming a Gaussian for the CIRFs of the mantle filter and assess the consequences for jerk occurrence times. We discuss the applicability and limitations of Backus' mantle filter theory in Section 4.

2 THEORY

2.1 Time constants

The magnetic field can be decomposed into toroidal-poloidal parts. In a solid mantle the poloidal scalar obeys the diffusion equation:

$$\frac{\partial \mathcal{P}(r,\theta,\phi,t)}{\partial t} = \frac{1}{\mu_0 \sigma(r)} \nabla^2 \mathcal{P}(r,\theta,\phi,t). \tag{2}$$

The poloidal scalar can be expanded in terms of spherical harmonics:

$$\mathcal{P}(r,\theta,\phi,t) = \sum_\ell \sum_m p_\ell^m(r,t) Y_\ell^m(\theta,\phi), \tag{3}$$

where $Y_\ell^m(\theta,\phi)$ are the Schmidt quasi-normalized spherical harmonics, $p_\ell^m(r,t)$ are the corresponding poloidal scalar coefficients, ℓ is the degree and m the order. The radial magnetic field at the CMB is given by:

$$B_r(c,t) = \frac{1}{c^2} \sum_{\ell,m} \ell(\ell+1) p_\ell^m(c,t). \tag{4}$$

Backus (1983) developed a theory in which the mantle behaves as a linear, causal and time invariant filter. The input signal is represented by a geomagnetic jerk, assumed to be a second-order impulse, simultaneous at the CMB. The output at the Earth's surface, $p_\ell^m(a,t)$, is calculated by the convolution between the CMB input, $p_\ell^m(c,t)$, and the following filters:

$$\begin{aligned} p_\ell^m(a,t) &= \mathcal{G}(\ell) F(\ell,t) * p_\ell^m(c,t) \\ &= \mathcal{G}(\ell) \int_{-\infty}^{\infty} F(\ell, t-t') p_\ell^m(c,t')\, \mathrm{d}t', \end{aligned} \tag{5}$$

where a is the Earth's radius ($a = 6371$ km), c is the core radius ($c = 3485$ km), ℓ is the harmonic degree, $\mathcal{G}(\ell) = \left(\frac{c}{a}\right)^{\ell+1}$ is the geometrical filter and $F(\ell,t)$ is the IRF representing the mantle filter. The IRF is only dependent on the mantle conductivity model (for more details see Appendix A). The *transfer function (TF)* represents the mantle filter in the frequency domain and may be calculated by the inverse Fourier transform of the IRF:

$$\tilde{F}(\omega) = \int_{-\infty}^{\infty} F(t) e^{i\omega t} \mathrm{d}t, \tag{6}$$

where from hereafter the tilde denotes TFs (for definition of all variables see Table 1).

The CIRF represents the mantle filter by considering the jerk amplitude at each location:

$$F_{\rm loc}(\theta,\phi,t) = \sum_{\ell=1}^{L} \mathcal{A}(\ell,\theta,\phi) F(\ell,t), \tag{7}$$

where $\mathcal{A}(\ell,\theta,\phi)$ is the amplitude at each location for each harmonic degree (see again Table 1). Locally, jerk amplitude is defined as the difference between the linear trends of the SV before and after the jerk (Pinheiro *et al.* 2011). For each degree, the amplitude is defined as the difference between the secular acceleration of the corresponding Gauss coefficients before and after the jerk (Pinheiro & Jackson 2008).

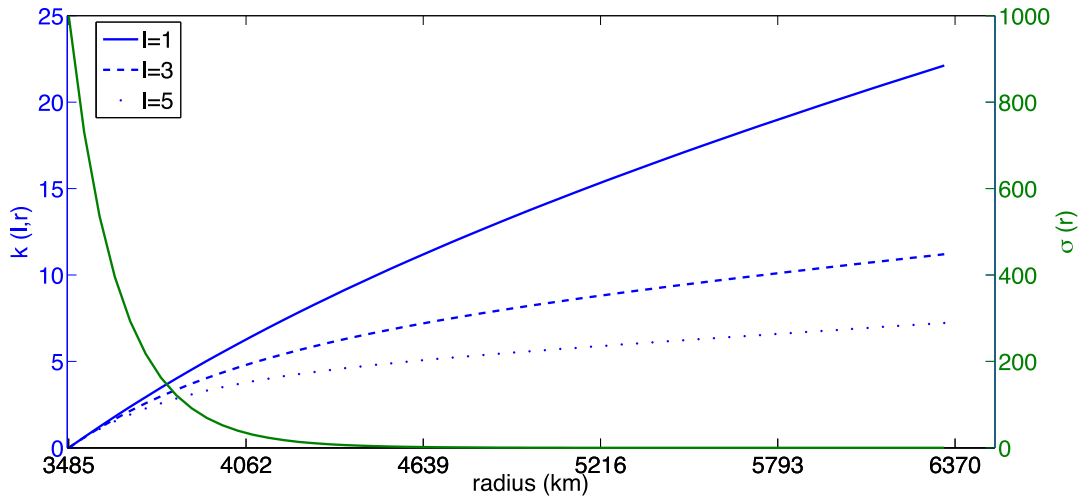

Figure 2. Kernels of different harmonic degrees (blue, eq. 14) and a radial profile of a mantle electrical conductivity model (green), both as functions of radial distance.

Two main constants characterize the mantle filter: the delay time τ and the smoothing time $(\beta_2)^2$. The delay time for each harmonic degree is independent of the location and calculated by the first moment of the IRF curves:

$$\tau(\ell) = \frac{1}{\tilde{F}(\ell, 0)} \int_{-\infty}^{\infty} F(\ell, t)\, t \, \mathrm{d}t. \tag{8}$$

Note that $\tau(\ell)$ is always positive, that is a jerk signal of a certain degree takes a finite positive time to diffuse from the CMB to the Earth's surface. Similarly, the delay time at a certain location is calculated directly by the first moment of the CIRF,

$$\tau_{\mathrm{loc}}(\theta, \phi) = \frac{1}{\tilde{F}_{\mathrm{loc}}(0)} \int_{-\infty}^{\infty} F_{\mathrm{loc}}(\theta, \phi, t)\, t \, \mathrm{d}t \tag{9}$$

or by the sum of weighted delay times for each harmonic degree (Backus 1983):

$$\tau_{\mathrm{loc}}(\theta, \phi) = \sum_{\ell=1}^{L} \alpha(\ell, \theta, \phi)\tau(\ell), \tag{10}$$

where $\alpha(\ell, \theta, \phi)$ is the ratio between the jerk amplitude for each harmonic degree and the sum of all amplitudes $\mathcal{A} = \sum_{\ell} \mathcal{A}(\ell)$:

$$\alpha(\ell, \theta, \phi) = \frac{\mathcal{A}(\ell, \theta, \phi)}{\mathcal{A}(\theta, \phi)}. \tag{11}$$

Note that $\alpha(\ell, \theta, \phi)$ may acquire positive or negative signs, reflecting the different possible jerk amplitude signs. As a result, the delay time at a certain location (10) may also be positive or negative. Finally, the smoothing time at a certain location $(\beta_2)^2_{\mathrm{loc}}(\theta, \phi)$ is defined as the second central moment of the CIRF curve:

$$(\beta_2)^2_{\mathrm{loc}}(\theta, \phi) = \int_{-\infty}^{\infty} \frac{F_{\mathrm{loc}}(\theta, \phi, t)(t - \tau_{\mathrm{loc}})^2}{\tilde{F}_{\mathrm{loc}}(0)} \mathrm{d}t. \tag{12}$$

2.2 Kernels

The jerk delay times for each harmonic degree, $\tau(\ell)$, may be expressed as a function of the radial electrical conductivity profile, $\sigma(r)$ by:

$$\tau(\ell) = \int_{c}^{a} \kappa(\ell, r)\sigma(r)\, \mathrm{d}r, \tag{13}$$

where the kernel is (Backus 1983):

$$\kappa(\ell, r) = \left(\frac{\mu_0}{2\ell + 1}\right) r \left[1 - \left(\frac{c}{r}\right)^{2\ell+1}\right], \tag{14}$$

and μ_0 is the magnetic permeability. Combining eqs (13) and (14) gives:

$$\tau(\ell) = \frac{\mu_0}{2\ell + 1} \int_{c}^{a} r \left[1 - \left(\frac{c}{r}\right)^{2\ell+1}\right] \sigma(r)\, \mathrm{d}r. \tag{15}$$

One way to better understand the mantle's filter behaviour is by interpreting eq. (13). We consider a generic 1-D radial mantle conductivity profile proposed by Lahiri & Price (1939):

$$\sigma(r) = \sigma_c \left(\frac{c}{r}\right)^{2\gamma+2}, \tag{16}$$

where σ_c is the electrical conductivity of the lowermost mantle and γ is a constant. The model shown in Fig. 2 simulates an extremely high mantle electrical conductivity ($\sigma_c = 1000\,\mathrm{S\,m^{-1}}$ and $\gamma = 3$) compared to previous estimates (e.g. Olsen 1999; Kuvshinov & Olsen 2006). In this figure, we plot kernels for different harmonic degrees that show (i) convergence to zero at the CMB, and (ii) kernels of lower degrees are larger and thus may generate larger delay times.

Jerk delay times, for each ℓ, are calculated by the area of the product of the two curves $\sigma(r)$ and $\kappa(\ell, r)$ as shown in Fig. 3(a). In this case ($\gamma = 3$), the lower mantle will mostly influence jerk delay times. The fraction of delay time originating below the D″ ranges between 13 and 20 per cent for the three harmonics shown in Fig. 3(a). These fractions are larger than the 10 per cent fraction of D″ depth, especially for the higher degrees. In addition, we define critical radius as the maximum value of the curves $\sigma(r)\kappa(\ell, r)$ for each harmonic degree, which we interpret as the radial distance from the CMB that mostly influences the jerk delay times. The curves in Fig. 3(a) peak at about $r = 4000$ km, just above the D″ layer. We calculated the critical radius for different radial profiles of the mantle electrical conductivity (by varying γ in eq. (16)), as shown in Fig. 3(b). This figure demonstrates that larger γ gives smaller critical radius. For $\gamma \geq 5$ the critical radius is well within the D″ layer. In addition, higher harmonic degrees have deeper critical radius.

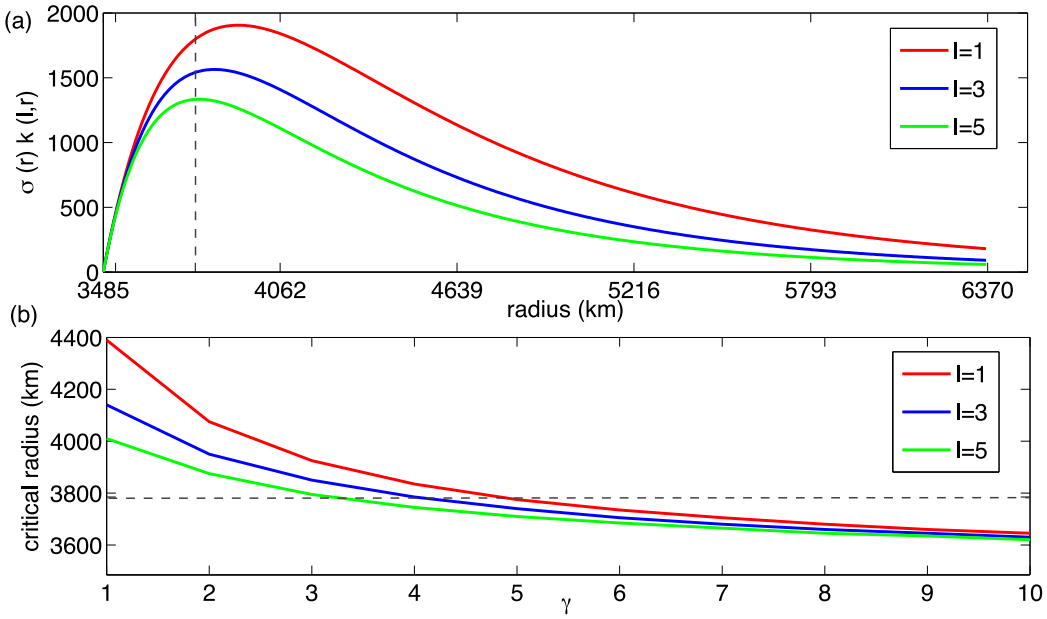

Figure 3. (a) Product between the radial profile of the electrical conductivity and the kernels for different harmonic degrees (integrand of eq. 13), as a function of radial distance. (b) Critical radius, or maximum values in the $\sigma(r)\kappa_\ell(r)$ curves, for different values of γ for different harmonic degrees. Vertical line in (a) and horizontal line in (b) denote an upper limit estimate of the D″ radius (see Schubert *et al.* 2001, and references therein). In (a), the fraction of delay time originating below the D″ is 13 per cent, 17 per cent and 20 per cent for $\ell = 1$, 3 and 5, respectively.

Table 2. Synthetic examples of delay times ($\tau(\ell)$ in yr), amplitudes ($\mathcal{A}(\ell, \theta, \phi)$ in nT yr^{-2}) and the amplitude ratios ($\alpha(\ell, \theta, \phi)$) at two arbitrary locations (θ_1, ϕ_1 and θ_2, ϕ_2) for each harmonic degree ℓ until the truncation degree $L = 3$.

ℓ	$\tau(\ell)$	$\mathcal{A}(\ell, \theta_1, \phi_1)$	$\alpha(\ell, \theta_1, \phi_1)$	$\mathcal{A}(\ell, \theta_2, \phi_2)$	$\alpha(\ell, \theta_2, \phi_2)$
1	3	4	0.1538	4	−0.6666
2	2	6	0.2308	6	−1.0000
3	1	16	0.6154	−16	2.6666
Total		26		−6	

3 HOW WELL MAY A GAUSSIAN REPRESENT THE MANTLE FILTER?

Backus (1983) applied a low-frequency approximation for the TF which allows approximating the CIRF by a Gaussian. This approximation fails when the delay time is negative which would mean earlier jerk occurrence at Earth's surface than on the CMB, and/or when the smoothing time is negative which would be the equivalent to sharper jerk behaviour at Earth's surface than on the CMB. Therefore, negative delay or smoothing times disable the use of Backus' theory to represent the mantle filter. To illustrate this point, synthetic examples of delay times at two arbitrary locations are presented in Table 2. The IRF of each harmonic degree $F(\ell, t)$ is represented by a Gaussian with a delay time (or first moment) that decreases with increasing harmonic degree. Each IRF curve is multiplied by each synthetic jerk amplitude, which results in the CIRF for each harmonic degree (eq. 7). The only difference between the two locations is the amplitude of $\ell = 3$ and therefore $\alpha(\ell, \theta, \phi)$ is also different (Table 2). The Gaussian is a good representation in location 1 where $\tau_{\rm loc}(\theta_1, \phi_1) = 1.54$ yr and $(\beta_2)^2_{\rm loc}(\theta_1, \phi_1) = 1.56$ yr^2 are both positive, but in location 2 it is impossible to represent the CIRF by a Gaussian since $\tau_{\rm loc}(\theta_2, \phi_2) = -1.33$ yr and $(\beta_2)^2_{\rm loc}(\theta_2, \phi_2) = -8.11$ yr^2 are negative.

We consider a more realistic scenario by adopting a generic 1-D radial mantle conductivity profile (Fig. 2). Using this model we calculate the IRFs for each harmonic degree $F(\ell, t)$. In addition, in order to calculate the CIRFs, a jerk amplitude model is needed. Jerk amplitudes were measured by fitting two straight-line segments to the Y component of the geomagnetic SV during the 1969 jerk based on the spherical harmonic model of Pinheiro *et al.* (2011), see their fig. 14d.

We calculated the CIRFs as well as the delay and smoothing times at 90 locations corresponding to magnetic observatories where the 1969 jerk was detected in the analysis of Pinheiro *et al.* (2011). For reference we considered median values of delay and smoothing times since some observatories presented anomalously large values that might bias an average. The median values of delay and smoothing times were found to be $\langle \tau_{\rm loc} \rangle = 6.67$ yr and $\langle (\beta_2)^2_{\rm loc} \rangle = 14.95$ yr. We display six locations corresponding to magnetic observatories that span the strength and limitations of Backus' methodology (Table 3). Observatories 2 and 3 are examples of positive delay and smoothing times close to the median values. Observatories 1 and 4 present smaller/larger delay and smoothing times, respectively. Observatories 5 and 6 are examples where Backus' filter theory cannot represent the CIRFs due to one or two negative time constants.

Fig. 4 shows the IRFs and CIRFs of observatories 2 and 5 obtained by the 1969 spherical harmonic model of Pinheiro *et al.* (2011). The area under the IRF curve represents the amplitude of the jerk for each ℓ. The first moment of each IRF curve represents the delay time, which is slightly different for each ℓ. The sum of all IRFs gives the CIRF for each observatory (eq. 7). Observatory 2 is an example of positive jerk amplitude, delay and smoothing times, its CIRF is positive at all times and therefore may be well represented by a Gaussian. In observatory 5 the amplitudes of different degrees almost cancel out and the resulting CIRF alternates signs with time and thus may not be represented by a Gaussian.

The Gaussian approximations of the CIRFs are calculated using the delay time as the first moment and the smoothing time as the variance (see eq. 1) of the Gaussian curves. Fig. 5 shows the CIRFs

Table 3. Number, code and location of six magnetic observatories for the 1969 jerk (Y component). The detection time of this jerk (t_0) was taken from Pinheiro *et al.* (2011). The amplitude ($\mathcal{A}$ in nT yr^{-2}), delay (τ in yr) and smoothing times (β_2^2 in yr^2) at the observatories are given.

n^o	Code	Latitude	Longitude	t_0	$\mathcal{A}$	τ	$(\beta_2)^2$
1	API	−13.80	188.23	1973.47	2.60	4.73	0.92
2	MBC	76.32	240.63	1974.27	1.14	6.02	12.42
3	CLF	48.02	2.27	1969.24	6.14	6.81	15.53
4	BJI	40.03	116.18	1970.28	−0.80	10.27	17.71
5	GUA	13.58	144.87	1966.21	0.01	152.15	−13998.89
6	MIR	−66.55	93.02	1971.00	0.22	−2.75	−122.23

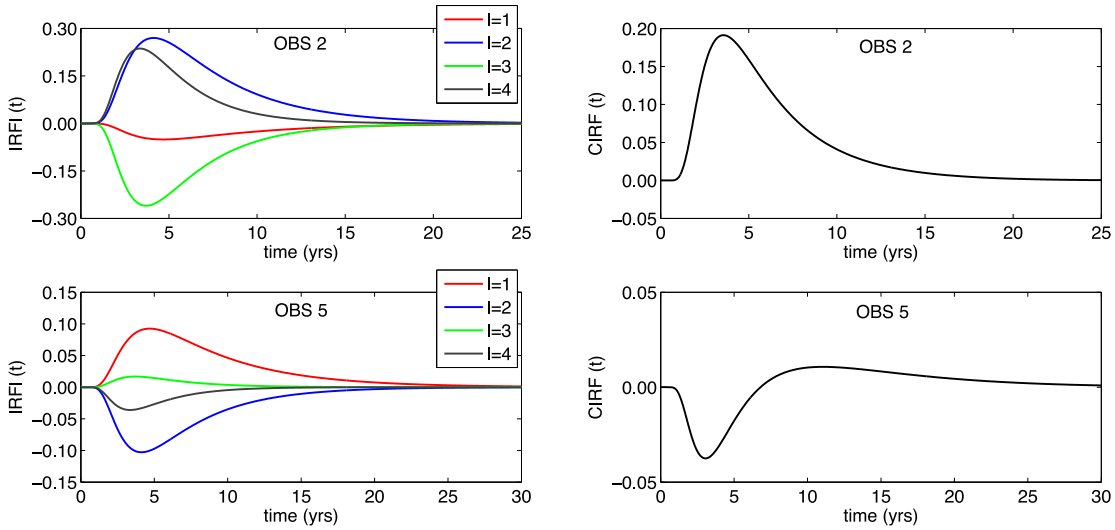

Figure 4. IRF of each harmonic degree for observatories 2 and 5 (left-hand panel). The sum of all IRFs gives the CIRF for each observatory (right-hand panel).

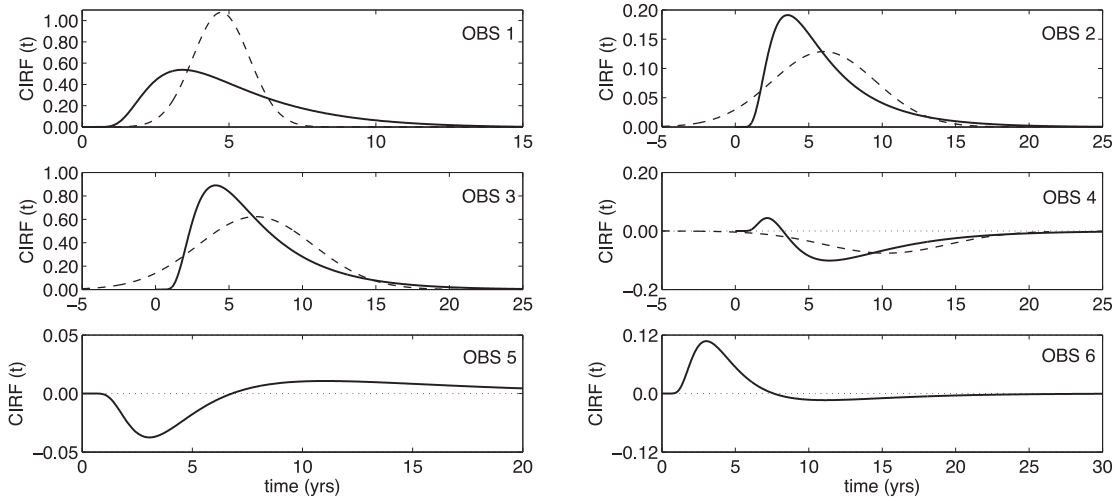

Figure 5. Composite IRF (solid line) calculated by the 1969 spherical harmonic model of Pinheiro *et al.* (2011) with a model of the radial profile of the electrical conductivity. The dashed line represents the Gaussian.

and their Gaussian approximations. It demonstrates the potential inadequacy of the Gaussian approximations for the CIRFs, due to three main reasons: (i) maximum values of Gaussian curves are dictated by its normalization and may disagree with the CIRFs; (ii) the asymmetric character of CIRFs and (iii) CIRFs might alternate signs, as in observatories 4–6. However, even in CIRFs that alternate signs, the Gaussian approximation may be possible when delay and smoothing times are positive. However, in observatories 5 and 6 the Gaussian representation is not possible because of the negative smoothing and/or delay times.

The reason for the negative smoothing times in observatories 5 and 6 is apparent in Fig. 6 where the integrands of eq. (12) are plotted. In the case of observatory 5 the area under the integrand curve is close to zero, leading to an unrealistically large delay time; In the other observatories the areas under the integrands are sufficiently different than zero and their corresponding delay times are therefore reasonable. Negative delay and/or smoothing times arise when the contributions of different degrees to the CIRF have distinctive delays and/or opposite amplitude signs. In situations where the CIRFs have slight opposite signs with respect to the peak but

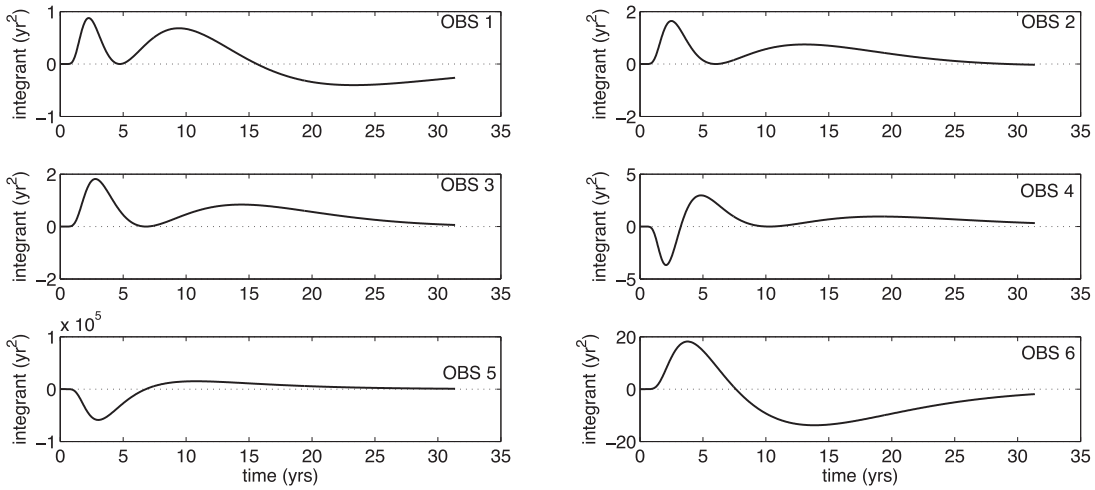

Figure 6. Integrands of the smoothing time constant of the six observatories shown in Table 4. Note that even a slightly sign alternating CIRF (OBS 5) might lead to a negative smoothing time.

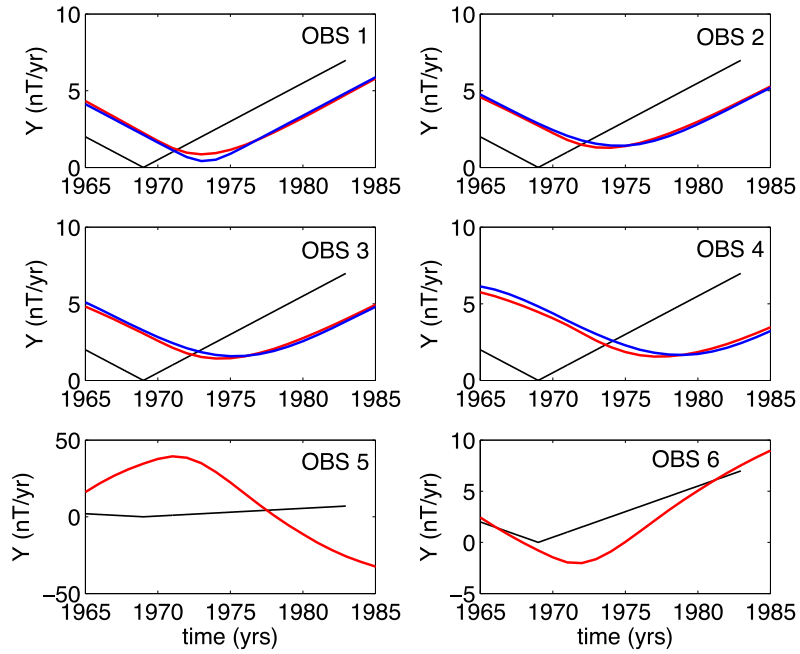

Figure 7. Convolution of an arbitrary jerk with $\mathcal{A} = 1$ (black line) with the CIRF (red line) and its Gaussian approximation (blue line) of the six observatories (Table 4). The Gaussian approximations of OBS 5 and 6 are not shown due to their negative time constants (Table 3).

for a long period (see Fig. 5 OBS 5 and OBS 6), negative delay and smoothing times might occur, since their integrands will enhance the opposite sign part.

Next, we convolve the input (jerk signal at the CMB) with the mantle filter (represented by the CIRF and its Gaussian) to obtain the output (jerk at the surface). In Fig. 7 we calculated the convolution of a simulated jerk with the Gaussian and with the CIRF in the observatories listed in Table 3. In order to analyse the model results in the same way as geomagnetic data is usually analysed, annual means where evaluated for both convolved CIRF and Gaussian. Note that the difference between the convolved CIRF and Gaussian (Fig. 7) is much smaller than the difference between the CIRF and the Gaussian prior to the convolution (Fig. 5). The curves were fitted using two straight line segments by a least-squares method (Pinheiro *et al.* 2011). The jerk occurrence time, defined as the intersect of the two segments, is different for the convolved CIRF and the Gaussian. Fig. 7 and Table 4 show that these differences are rather small in observatories 1 and 2 but become significant in observatories 3 and 4, a consequence of the temporal offset of the Gaussian approximation with respect to the CIRF in these locations. As mentioned above, Gaussians cannot be calculated for

Table 4. Jerk occurrence times detected using a least-squares fit of the convolution between annual means of CIRF and Gaussian with a jerk.

n^o	Code	CIRF jerk time	Gaussian jerk time	Difference
1	API	1973.47	1973.34	−0.13
2	MBC	1974.27	1974.66	0.39
3	CLF	1974.58	1975.48	0.90
4	BJI	1977.36	1978.40	1.03
5	GUA	1970.81	–	–
6	MIR	1971.60	–	–

Table 5. Sensitivity of convolution depending on two spherical harmonic models for the 1969 jerk (Y component), Pinheiro *et al.* (2011) and Le Huy *et al.* (1998), and three radial profiles of the mantle electrical conductivity (varying σ_c and γ). The statistics of the differences between the occurrence times of the convolved jerk with the CIRFs and Gaussians of the 90 observatories are calculated. Percentages of CIRFs that are well represented by Gaussians ($\Delta < 0.5$ yr), CIRFs that are not well represented by Gaussians ($\Delta > 0.5$ yr) and CIRFs that could not be represented by Gaussians because of negative delay and/or smoothing times are given.

Jerk model	σ_c (S m^{-1})	γ	$\Delta < 0.5$	$\Delta > 0.5$	No fit	Mean
Pinheiro *et al.* (2011)	1000	3	13	81	6	0.86
Pinheiro *et al.* (2011)	3000	10	0	94	6	1.15
Pinheiro *et al.* (2011)	3000	11	0	97	3	1.36
Le Huy *et al.* (1998)	1000	3	14	74	11	0.81
Le Huy *et al.* (1998)	3000	10	0	92	8	1.14
Le Huy *et al.* (1998)	3000	11	0	93	7	1.33

observatories 5 and 6 due to their negative time constants. We repeated this calculation for all 90 observatories. We arbitrarily chose $\Delta = 0.5$ yr as a critical value distinguishing adequate and inadequates Gaussian approximations.

We calculate global statistics of occurrence times differences. Using the jerk morphology model of Pinheiro *et al.* (2011) and a relatively flat mantle electrical conductivity model (first line in Table 5), we found in 13 per cent of the locations that the difference between the occurrence time of the convolved jerk with the CIRF and with the Gaussian was smaller than 0.5 yr, that is the Gaussian approximation is adequate. In most cases (81 per cent of the locations) this difference was greater than $\Delta = 0.5$ yr, that is the Gaussian approximation is not adequate. In the remaining few 6 per cent of the locations negative time constants prohibited the use of the Gaussian approximation. We also test the sensitivity of our results to different jerk morphology and mantle electrical conductivity models (Table 5). In most observatories (74–97 per cent) we found relatively large differences between the convolved jerks with CIRFs and with Gaussians, while in less than 14 per cent this difference was smaller than 0.5 yr and in less than 11 per cent it was impossible to calculate Gaussians due to negative delay and/or smoothing times.

4 DISCUSSION

Geomagnetic jerks generated in the core propagate through the mantle before arriving at the Earth's surface. Because of the electrical conductivity of the mantle, the observed jerk at the surface is a delayed and smoother version of the original jerk in the core. Backus (1983) developed a theory that relates radial profiles of the mantle's electrical conductivity with jerk delay times. This relation, expressed by the kernels, varies for each harmonic degree and as a function of the radial distance from the CMB. Analysis of the kernels shows convergence to zero at the CMB and that lower harmonic degrees are more delayed. Using a generic electrical conductivity model, we demonstrated that deeper layers of the lower mantle affect higher harmonic degrees. Moreover, despite the fact that the kernels are zero on approach to the CMB (Fig. 2), the lower mantle electrical conductivity governs jerk delay times (Fig. 3).

In this paper, we examined two main issues of the mantle filter theory: (i) the limitation of the Gaussian approximation for calculating CIRFs and its consequences for jerk occurrence times, and (ii) the application of the linear relation between jerk delay times and a mantle electrical conductivity model to geomagnetic data. The low-frequency approximation is not valid when the delay and/or smoothing times are negative. We showed that negative smoothing times may be caused by alternating sign CIRFs due to geomagnetic jerks harmonic mixing for a given mantle electrical conductivity model. An alternating sign CIRF curve may be generated by different jerk amplitudes of different harmonic degrees (Fig. 4).

We calculated the CIRFs of locations corresponding to 90 magnetic observatories, using the same radial profile of mantle conductivity and the amplitude jerk model of Pinheiro *et al.* (2011). We classified three scenarios (Figs 5 and 7): (i) CIRFs that are well represented by Gaussians, (ii) CIRFs that are not well represented by Gaussians but have positive time constants and (iii) CIRFs that could not be represented by Gaussians because of negative delay and/or smoothing times. Negative smoothing times might occur when an opposite sign part of the CIRF is enhanced at times far from the jerk occurrence (see eq. 12 and OBS 5 and OBS 6 in Fig. 6).

We compared the statistics of the convolution using different jerk morphologies (for the same mantle electrical conductivity model) and using different electrical conductivity models (for the same jerk morphology model). We found low sensitivity of the statistics to the different models which may indicate that these results are robust. In most observatories the time constants are positive, but the difference between the occurrence times often exceeds 0.5 yr. This means that the mantle filter theory can be implemented in most cases, but it does not provide highly accurate occurrence times often enough. It is important to note however that the latter result depends strongly on the specific choice of the acceptable occurrence times difference Δ.

Convolving the input jerks with the CIRFs demonstrates that the difference between the jerk occurrence times is not significant where the Gaussian approximation is adequate, but inadequate Gaussian approximation might cause differences as large as 1 yr. Pinheiro & Jackson (2008) showed that jerk differential delay times of about 2 yr may be caused by a 1-D mantle electrical conductivity model. In data analysis, jerk differential delays are found to be also of the order of 2 yr, but in some locations it may reach around 6 yr (Alexandrescu *et al.* 1996; Le Huy *et al.* 1998; Pinheiro *et al.* 2011). Therefore, the differences of more than 0.5 yr in jerk occurrence times that we detected by comparing CIRFs and Gaussians may be significant in terms of accurately inferring mantle conductivity models.

As shown in Table 5 the applicability of the Gaussian approximation may somewhat depend on the jerk morphology model. We compared the models of Le Huy *et al.* (1998) and Pinheiro *et al.* (2011) for the Y component of the 1969 jerk. In a more recent

study, Brown *et al.* (2013) identified jerks in magnetic observatory monthly mean data using temporal sliding windows. Their approach provides histograms of jerk occurrence times based on minimal *a priori* information. Although Table 5 shows low sensitivity to the jerk morphology model, overall it is worthwhile exploring more models for example that of Brown *et al.* (2013).

It is interesting to note that despite rather large misfits between CIRFs and Gaussians (Fig. 5), the fits between their corresponding convolved curves are significantly superior (Fig. 7). This demonstrates that even when the Gaussian does not seem to represent well the CIRF, it suffices to have positive and similar delay and smoothing times to well reproduce the jerk's behaviour. This may be seen as an empirical support to the use of mantle filter theory.

Backus (1983) demonstrated that negative smoothing time occurs due to harmonic mixing. Alternatively, he proposed the influence of external sources. Courtillot & Le-Mouel (1984) demonstrated this scenario by constructing a synthetic Y component SV by two continuous parabolas with a jump in the second derivative in 1969. They added a synthetic sunspot signal using a solar cycle period of 10 nT amplitude, obtaining $(\beta_2)^2 = -2.7\ \mathrm{yr}^2$.

The mantle filter theory may provide insights into the mantle's electrical conductivity by exploring the possible radial profiles which reproduce the observed jerk differential delays times. Such a search may be pursued by considering a wide range of mantle electrical conductivity models and calculating misfits between jerk differential delays obtained by the data and by the theory. Note that Backus' mantle filter theory considers only 1-D radial mantle electrical conductivity profiles; to incorporate lateral heterogeneities, alternative time-domain methods should be applied (Velímský & Martinec 2005; Velímský *et al.* 2006). The duration of a jerk or smoothing time in observatory data is not well defined (although attempts have been made, see Nagao *et al.* 2003), since jerks' behaviour is not simple, but it may be reflected in the error bars of the jerk occurrence times. However, the time in which the linear trend of the SV changes sign (or jerk duration) usually does not last more than 2 yr. This data information may be used to provide upper bounds on mantle electrical conductivity models.

An alternative way to infer the time constants is to convolve a synthetic jerk with CIRFs and calculate the delay and smoothing times in the convolved jerk (as shown in Fig. 7) in the same way that an observatory data set is treated. In this way the Gaussian approximation is abandoned and as a result some alternating sign CIRFs (that were excluded with the Gaussian approximation) can be considered (e.g. OBS 6). Nevertheless, we recall that using the Gaussian approximation is in general advantageous since it provides analytical expressions for the kernels and the subsequent time constants.

Jerks detection and analysis will soon be greatly improved thanks to the three satellites of the Swarm mission that were launched by the European Space Agency in November 2013. These satellites currently monitor the Earth's magnetic field with unprecedented high-quality and globally distributed data set (Friis-Christensen *et al.* 2006). The expected data will provide a better characterization of the geomagnetic SV. Specifically relevant to this study, Swarm data may allow improving determination of jerk occurrence times and inferring jerk duration times. The influence of the external field on the SV data will also be better modelled by the Swarm data set. Overall, a better understanding of the applicability of the mantle filter theory in conjunction with new magnetic satellite data may shed light on the structure of the deep mantle and provide insights about the physical mechanisms responsible for geomagnetic jerks in the core.

ACKNOWLEDGEMENTS

This research was supported by the Centre National d'Etudes Spatiales (CNES), by CAPES (Coordenação de Aperfeiçoamento de Pessoal de Nível Superior – Proc nº BEX 2498/13-8) and by a Dorothy Hodgkin Postgraduate Award from Research Councils UK. We thank François Civet for insightful discussions. We thank two anonymous reviewers and the editor for their suggestions that greatly improved this paper.

REFERENCES

Achache, J., Courtillot, J., Ducruix, J. & Le Mouël, J.-L., 1980. The late 1960's secular variation impulse: further constraints on deep mantle conductivity, *Phys. Earth planet. Int.,* **23,** 72–75.

Alexandrescu, M., Gilbert, D., Hulot, G., Le, Mouël, J.-L. & Saracco, G., 1996. Worldwide wavelet analysis of geomagnetic jerks, *J. geophys. Res.,* **101**(B10), 21 975–21 994.

Alexandrescu, M., Gilbert, D., Le, Mouël J.-L., Hulot, G. & Saracco, G., 1999. An estimate of average lower mantle conductivity by wavelet analysis of geomagnetic jerks, *J. geophys. Res.,* **104**(B8), 17 735–17 745.

Backus, G.E., 1983. Application of mantle filter theory to the magnetic jerk of 1969, *Geophys. J. R. astr. Soc.,* **74,** 713–746.

Bloxham, J., Zatman, S. & Dumberry, M., 2002. The origin of geomagnetic jerks, *Nature,* **420**(6911), 65–68.

Brown, W.J., Mound, P.W. & Livermore, P.W., 2013. Jerks abound: an analysis of geomagnetic observatory data from 1957 to 2008, *Phys. Earth planet. Int.,* **223,** 62–76.

Chulliat, A., Thébault, E. & Olsen, N., 2010. Core field acceleretion pulse as a common cause of the 2003 and 2007 geomagnetic jerks, *Geophys. Res. Lett.,* **37,** L07301, doi:10.1029/2009GL042019.

Constable, S., 2007. *Geomagnetism in Treatise on Geophysics,* Vol. 5, pp. 237–276, Elsevier.

Courtillot, V. & Le-Mouel, J.-L., 1984. Geomagnetic secular variation impulses, *Nature,* **311,** 709–716.

Courtillot, V., Ducruix, J. & Le-Mouel, J.-L., 1978. Sur une accélération récente de la variation séculaire du champ magnétique terrestre, *C. R. Acad. Sci. Paris,* **287,** 1095–1098.

Friis-Christensen, E., Luhr, H. & Hulot, G., 2006. Swarm: a constellation to study the earth's magnetic field, *Earth Planets Space,* **58,** 351–358.

Holme, R. & de Viron, O., 2005. Geomagnetic jerks and a high resolution length-of-day profile for core studies, *Geophys. J. Int.,* **160,** 435–439.

Holme, R. & de Viron, O., 2013. Characterization and implications of intradecadal variations in length of day, *Nature,* **499,** 202–204.

Kuvshinov, A. & Olsen, N., 2006. A global model of mantle conductivity derived from 5 years of CHAMP, Ørsted, and SAC-C magnetic data, *Geophys. Res. Lett.,* **33**, L18301, doi:10.1029/2006GL027083.

Kuvshinov, A., Utada, D., Avdeev, D. & Koyama, T., 2005. 3-D modelling and analysis of Dst C-responses in the North Pacific Ocean region, revisited, *Geophys. J. Int.,* **160,** 505–526.

Lahiri, B.N. & Price, A.T., 1939. Electromagnetic induction in non-uniform conductors, and the determination of the conductivity of the earth from terrestrial magnetic variations, *Phil. Trans. R. Soc.,* **A237,** 509–540.

Le Huy, M., Alexandrescu, M., Hulot, G. & Le Mouël, J.-L., 1998. On the characteristics of successive geomagnetic jerks, *Earth Planets Space,* **50,** 723–732.

Malin, S.R.C. & Hodder, B.M., 1982. Was the 1970 geomagnetic jerk of internal or external origin?, *Nature,* **296,** 726–728.

Mandea, M., Bellanger, E. & Le Mouël, J.-L., 2000. A geomagnetic jerk for the end of the 20th century?, *Earth planet. Sci. Lett.,* **183,** 369–373.

McDonald, L.K., 1957. Penetration of the geomagnetic secular field through a mantle with variable conductivity, *J. geophys. Res.,* **62**(1), 117–140.

Murakami, M., Hirose, K., Kawamura, K., Sata, N. & Ohishi, Y., 2004. Post-perovskite phase transition in $MgSiO_3$, *Science,* **304,** 855–858.

Nagao, H., Iyemori, T., Higuchi, T. & Araki, T., 2003. Lower mantle conductivity anomalies estimated from geomagnetic jerks, *J. geophys. Res.,* **108**(B5), 2254, doi:10.1029/2002JB0011786.

Ohta, K., Onoda, S., Hirose, K., Sinmyo, R., Sata, N., Ohishi, Y. & Yasuhara, A., 2008. The electrical conductivity of post-perovskite in the Earth's D″ layer, *Science,* **320,** 89–91.

Olsen, N., 1998. Estimation of *C*-responses (3h to 720h) and the electrical conductivity of the mantle beneath Europe, *Geophys. J. Int.,* **133,** 298–308.

Olsen, N., 1999. Long-period (30 days – 1 year) electromagnetic sounding and the electrical conductivity of the lower mantle beneath Europe, *Geophys. J. Int.,* **138,** 179–187.

Olsen, N. & Mandea, M., 2007. Investigation of a secular variation impulse using satellite data: the 2003 geomagnetic jerk, *Earth Planets Space,* **255,** 94–105.

Olsen, N. & Mandea, M., 2008. Rapidly changing flows in the Earth's core, *Nature Geosci.,* **1,** 390–394.

Pinheiro, K. & Jackson, A., 2008. Can a 1D mantle electrical conductivity model generate magnetic jerk differential time delays?, *Geophys. J. Int.,* **173**(3), 781–792.

Pinheiro, K., Jackson, A. & Finlay, C.C., 2011. Measurements and uncertainties of the occurrence time of the 1969, 1978, 1991, and 1999 geomagnetic jerks, *Geochem. Geophys. Geosyst.,* **12**(10), doi:10.1029/2011GC003706.

Runcorn, S.K., 1955. The electrical conductivity of the earth's mantle, *Tran. Am. geophys. Un.,* **36**(2), 191–198.

Schubert, G., Turcotte, D.L. & Olson, P., 2001. *Mantle Convection in the Earth and Planets,* Cambridge University Press.

Semenov, A. & Kuvshinov, A., 2012. Global 3-D imaging of mantle electrical conductivity based on inversion of observatory C-responses—II. Data analysis and results, *Geophys. J. Int.,* **191**, doi:10.1111/j.1365–246X.2012.05665.x.

Silva, L. & Hulot, G., 2012. Investigating the 2003 geomagnetic jerk by simultaneous inversion of the secular variation and acceleration for both the core flow and its acceleration, *Phys. Earth planet. Int.,* **189–199,** 28–50.

Tarits, P. & Mandea, M., 2010. The heterogeneous electrical conductivity structure of the lower mantle, *Phys. Earth planet. Int.,* **183,** 115–125.

Velímský, J. & Finlay, C.C., 2011. Effect of a metallic core on transient geomagnetic induction, *Geochem. Geophys. Geosyst.,* **12**(5), doi:10.1029/2011GC003557.

Velímský, J. & Martinec, Z., 2005. Time-domain, spherical harmonic-finite element approach to transient three-dimensional geomagnetic induction in a spherical heterogeneous earth, *Geophys. J. Int.,* **161,** 81–101.

Velímský, J., Martinec, Z. & Everett, M.E., 2006. Electrical conductivity in the earth's mantle inferred from champ satellite measurements—I. Data processing and 1-D inversion, *Geophys. J. Int.,* **166,** 529–542.

Wardinski, I., Holme, R., Asari, S. & Mandea, M., 2008. The 2003 geomagnetic jerk and its relation to the core surface flows, *Earth planet. Sci. Lett.,* **267,** 468–481.

APPENDIX A: TIME CONSTANTS

The effect of the mantle filter is to delay and smooth the original signal generated at the CMB. The delay time is calculated by the first moment of the IRF curve. The smoothing time is calculated by the second central moment, or variance, of a Gaussian curve. The delay time is directly proportional to electrical conductivity and inversely proportional to the harmonic degree, while the smoothing time depends strongly on the mixing of harmonics.

The exponential of eq. (6) can be expanded into power series,

$$\tilde{F}(\omega) = \int_{-\infty}^{\infty} F(t) \sum_{n=0}^{\infty} \frac{1}{n!} (\imath \omega t)^n \mathrm{d}t, \tag{A1}$$

where n is the nth ordinary moment. The area under the IRF curve is expressed by:

$$\tilde{F}(0) = \int_{-\infty}^{\infty} F(t)\, \mathrm{d}t. \tag{A2}$$

Substituting eq. (A2) into eq. (A1):

$$\tilde{F}(\omega) = \tilde{F}(0) \sum_{n=0}^{\infty} \frac{1}{n!} (\imath \omega \tau_n)^n, \tag{A3}$$

where $(\tau_n)^n$ is the ordinary nth moment given by:

$$(\tau_n)^n = \frac{1}{\tilde{F}(0)} \int_{-\infty}^{\infty} F(t) t^n \mathrm{d}t. \tag{A4}$$

The delay time is given by the first moment ($n = 1$):

$$\tau = \frac{1}{\tilde{F}(0)} \int_{-\infty}^{\infty} F(t) t \ \mathrm{d}t, \tag{A5}$$

However, in order to calculate the delay time in different locations we must consider the CIRF (Pinheiro & Jackson 2008):

$$\tau_{\mathrm{loc}}(\theta, \phi) = \frac{1}{\mathcal{A}(\theta, \phi)} \int_{-\infty}^{\infty} F_{\mathrm{loc}}(\theta, \phi, t)\ t\ \mathrm{d}t, \tag{A6}$$

where $\mathcal{A}$ represents the sum of jerk amplitudes of all degrees and orders: $\mathcal{A}(\theta, \phi) = \sum_\ell \mathcal{A}_\ell(\theta, \phi)$. Since:

$$F_{\mathrm{loc}}(\ell, \theta, \phi, t) = \mathcal{A}(\ell, \theta, \phi) F(\ell, t), \tag{A7}$$

then:

$$\tau_{\mathrm{loc}}(\theta, \phi) = \frac{1}{\mathcal{A}(\theta, \phi)} \sum_{\ell=1}^{L} \sum_{m=0}^{\ell} \mathcal{A}(\ell, \theta, \phi) \int_{-\infty}^{\infty} F(\ell, t)\ t\ \mathrm{d}t, \tag{A8}$$

and since $\tau(\ell) = \int_{-\infty}^{\infty} F(\ell, t)\ t\ \mathrm{d}t$:

$$\tau_{\mathrm{loc}}(\theta, \phi) = \frac{1}{\mathcal{A}(\theta, \phi)} \sum_{\ell} \tau(\ell) \mathcal{A}(\ell, \theta, \phi). \tag{A9}$$

If we consider $\alpha(\ell, \theta, \phi) = \frac{\mathcal{A}(\ell, \theta, \phi)}{\mathcal{A}(\theta, \phi)}$ then eq. (A9) becomes:

$$\tau_{\mathrm{loc}}(\theta, \phi) = \sum_{\ell} \alpha(\ell, \theta, \phi) \tau(\ell). \tag{A10}$$

Eq. (A10) is used to calculate jerk delay times in different locations. The smoothing time is calculated by the second central moment, which corresponds to the variance of a Gaussian:

$$(\beta_2)^2 = \int_{-\infty}^{\infty} \frac{F(t)(t - \tau)^2}{\tilde{F}(0)} \mathrm{d}t. \tag{A11}$$

There are two general equations for the nth central moment, given by Backus (1983):

$$(\beta_n)^n = \frac{1}{\tilde{F}(0)} \int_{-\infty}^{\infty} F(t)(t - \tau)^n \mathrm{d}t. \tag{A12}$$

and

$$(\beta_n)^n = \sum_{m=0}^{n} (-1)^{n-m} \frac{n!}{(n-m)!m!} \tau_m^m \tau^{n-m}. \tag{A13}$$

By setting $n = 2$ in eq. (A13):

$$(\beta_2)^2 = -\tau^2 + \tau_2^2, \tag{A14}$$

and the general equation for expressing central moments as functions of first moments is written as:

$$(\beta_n)^n = -\tau^n + \tau_n^n. \tag{A15}$$

APPENDIX B: LOW FREQUENCY APPROXIMATION

The mantle filter theory proposed by Backus (1983) has the advantage to provide an analytical linear relation between jerk delay

times and radial profiles of the mantle's electrical conductivity. In this appendix we aim to clarify how the IRFs and CIRFs may be approximated by a Gaussian. Backus (1983) defined:

$$\tilde{F}^{\dagger}(t) = F(t-\tau) \tag{B1}$$

and therefore, $\tilde{F}(0) = \tilde{F}^{\dagger}(0)$ because:

$$\int_{-\infty}^{\infty} F(t)\,\mathrm{d}t = \int_{-\infty}^{\infty} F(t-\tau)\,\mathrm{d}t.$$

By the general definition of central moments (eq. A12) it is possible to notice that the central moments of $\frac{F(t)}{\tilde{F}(0)}$ are the ordinary moments of $\frac{F^{\dagger}(t)}{\tilde{F}(0)}$:

$$(\beta_n)^n = \frac{1}{\tilde{F}(0)} \int_{-\infty}^{\infty} F^{\dagger}(t) t^n \mathrm{d}t. \tag{B2}$$

Since

$$\tilde{F}(\omega) = \tilde{F}(0) \sum_{n=0}^{\infty} \frac{1}{n!} (\imath\omega\tau_n)^n, \tag{B3}$$

then

$$\tilde{F}^{\dagger}(\omega) = \tilde{F}(0) \sum_{n=0}^{\infty} \frac{1}{n!} (\imath\omega\beta_n)^n. \tag{B4}$$

We can also express $\tilde{F}^{\dagger}(\omega)$ as a function of $\tilde{F}(\omega)$:

$$\begin{aligned}\tilde{F}^{\dagger}(\omega) &= \tilde{F}(\omega) e^{-\imath\omega\tau} \\ &= \tilde{F}(0) \sum_{n=0}^{\infty} \frac{1}{n!} (\imath\omega(\tau_n - \tau))^n \\ &= \tilde{F}(0) \sum_{n=0}^{\infty} \frac{1}{n!} (\imath\omega\beta_n)^n \end{aligned} \tag{B5}$$

Backus (1983) defines real functions $\tau(\omega)$ and $\tau^{\dagger}(\omega)$ from the equations:

$$\tilde{F}(\omega) = |\tilde{F}(\omega)| e^{\imath\omega\tau(\omega)} \tag{B6}$$

and

$$\tilde{F}^{\dagger}(\omega) = |\tilde{F}^{\dagger}(\omega)| e^{\imath\omega\tau^{\dagger}(\omega)}. \tag{B7}$$

Comparing eqs (B5) and (B7)

$$\tau(\omega) = \tau + \tau^{\dagger}(\omega). \tag{B8}$$

Next, we expand eq. (B5) in Taylor series:

$$\begin{aligned}\frac{\tilde{F}^{\dagger}(\omega)}{\tilde{F}(0)} &= \sum_{n=0}^{\infty} \frac{1}{n!} (\imath\omega\beta_n)^n \\ &= -\frac{1}{2}(\beta_2)^2\omega^2 + \frac{1}{4}(\beta_2)^4\omega^4 + \frac{1}{24}(\beta_4)^4\omega^4 + \cdots \end{aligned}$$

and

$$\tau^{\dagger}(\omega) = -\frac{1}{6}(\beta_3)^3\omega^2 + \cdots \tag{B9}$$

Since $|\tilde{F}(\omega)| = |\tilde{F}^{\dagger}(\omega)|$, then:

$$\tilde{F}(\omega) = \tilde{F}(0) e^{\imath\omega\tau + 1/2(\imath\omega\beta_2)^2 + 1/6(\imath\omega\beta_3)^3 + \cdots} \tag{B10}$$

If we neglect higher powers than ω^3 in eq. (B10) then

$$\tilde{F}(\omega) \approx \tilde{F}(0) e^{\imath\omega\tau} e \frac{-\omega^2(\beta_2)^2}{2} \tag{B11}$$

and as result $\frac{\tilde{F}(\omega)}{\tilde{F}(0)}$ can be represented by a Gaussian when $(\beta_2)^2 > 0$.